ACS APPLIED MATERIALS & INTERFACES

www.acsami.org

Research Article

Tailoring a Hybrid Functional Layer for Mg Metal Anodes in Conventional Electrolytes with a Low Overpotential

Yichao Zhuang, Dongzheng Wu, Fei Wang, Yaoqi Xu, Jing Zeng,* and Jinbao Zhao*

Cite This: https://doi.org/10.1021/acsami.2c11911

Read Online

ACCESS | Metrics & More | Article Recommendations | Supporting Information

ABSTRACT: The development of high-voltage Mg metal batteries is hampered by the incompatibility between a Mg metal anode and conventional electrolyte, leading to a high overpotential for Mg plating/stripping processes. In this work, we tailored a hybrid functional layer consisting of Bi/$MgCl_2$/polytetrahydrofuran (PTHF) by an in situ THF polyreaction during the reaction of the Mg anode with $BiCl_3$ solution. The introduction of PTHF inhibits the growth of Bi particles and fills the layer interstice with $MgCl_2$-containing PTHF, improving the structural integrity of the functional layer and insulation between the electrolyte and Mg anode. As a result, compared to a simply modified Bi/$MgCl_2$ layer, the Bi/$MgCl_2$/PTHF functional layer exhibits a lower polarization voltage of 0.25 V and longer cycling life of more than 2000 h at 0.1 mA cm^{-2}. Mechanism analysis shows that Mg is plated on the surface of Bi particles within the layer. The Mo_6S_8/Mg full battery with the hybrid functional layer achieved a low voltage hysteresis of ~0.25 V and long cycling life over 500 cycles at 50 mA g^{-1}. This work provides a facile and effective hybrid functional layer strategy to realize Mg metal batteries in conventional electrolytes.

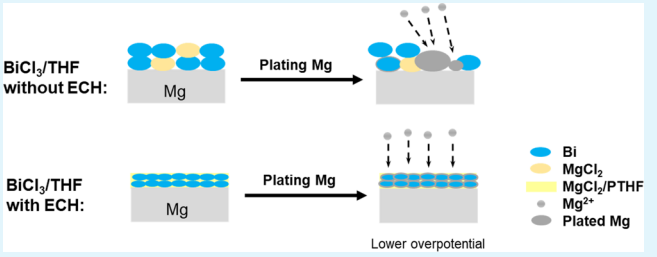

KEYWORDS: *Mg metal battery, Mg deposition, Mg metal anode, conventional electrolyte, hybrid functional layer*

1. INTRODUCTION

Mg metal batteries, as one of the most promising post-lithium batteries,[1−3] have attracted increasing attention owing to their high safety and low cost. For example, Mg is more abundant and cheaper compared to Li, which is helpful for large-scale applications. More importantly, a Mg metal anode possesses a low potential of −2.37 V vs standard hydrogen electrode (SHE) as well as a high specific mass capacity (2205 mAh g^{-1}) and volume capacity (3833 mAh cm^{-3}), showing great potential to achieve high-voltage Mg metal batteries with high energy density.[4−9] However, Mg metal batteries still have a long way to achieve commercial application, and one of the major sticking points is the lack of an appropriate electrolyte system compatible with both the anode and cathode simultaneously.[10−12] The current developed electrolytes that are compatible with Mg metal still show several limitations in Mg metal batteries. For instance, the most studied nonaqueous halo-aluminate electrolytes, such as all-phenyl complex or dichloro complex solutions, are not suitable for a high-voltage cathode due to the low oxidation potential,[13,14] high disassociation energy of Mg−Cl bond,[15,16] and Cl^- corrosion.[17,18] As for the electrolytes such as $Mg(CB_{11}H_{12})_2$/tetraglyme, their complex and high cost synthesis process need to be considered for commercialization.[19,20] Conventional electrolytes that are similar to the electrolyte for Li-ion batteries, such as $Mg(PF_6)_2$ or $Mg(TFSI)_2$ dissolved in ether, ester, or nitrile solvents, possess relatively high oxidation potential and good compatibility with a high-voltage cathode, and their production process can also refer to the existing Li-ion battery electrolyte, making it a promising electrolyte for high-voltage Mg metal batteries.[21−24] With these electrolytes, however, Mg metal tends to exhibit side reactions with anions or solvents and to form a passivation film on the surface of the Mg anode.[25−27] Unlike the Li^+ conductive solid electrolyte interphase (SEI) formed on Li metal, the passivation film on Mg metal conducts neither electrons nor Mg^{2+} ions, resulting in irreversible plating/stripping of Mg and failure of Mg metal batteries.[10,28,29] Therefore, it is an important task for Mg metal batteries to realize reversible Mg plating/stripping in conventional electrolytes through novel strategies.

To date, researchers have made much progress in realizing reversible Mg plating/stripping in conventional electrolytes. One of the major research directions is modifying the solvation shell structure of Mg^{2+} through altering the electrolyte composition, such as $MgCl_2$,[30] $Mg(BH_4)_2$,[31] methoxyethylamine chelants,[32] trimethyl phosphate[33] as an additive, or $Mg(TFSA)_2$[34] as an electrolyte salt, which has been proven to

Received: July 5, 2022
Accepted: September 29, 2022

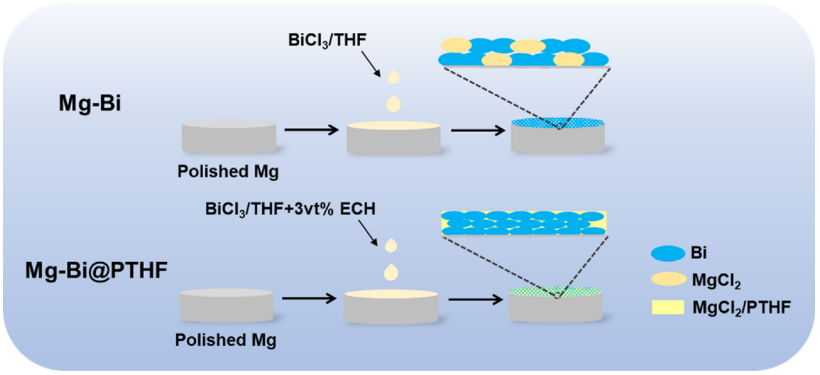

Figure 1. Preparation and Mg plating process of Mg-Bi and Mg-Bi@PTHF electrodes.

have a tremendous effect on realizing reversible Mg plating/stripping. Tailoring the functional layer on the Mg anode surface is also an effective way to address the anode/electrolyte incompatibility and high-voltage cathode limitation simultaneously.[35,36] For example, Chunmei et al. creatively engineered an artificial interphase interfacial film, which consisted of PAN and $Mg(CF_3SO_3)_2$ on the surface of Mg powder, achieving highly reversible Mg chemistry in conventional electrolytes for the first time;[37] Zuo et al. immersed Mg metal in LiTFSI +$AlCl_3$/tetraglyme solution, and a Mg^{2+} conductive SEI containing a large amount of $MgCl_2$, MgF_2, and MgS was formed on the Mg surface eventually;[38] Johnson et al. suggested a route to a low overpotential and stable interphase formed on Mg metal during cycling in $Mg(TFSI)_2$-tetraglyme electrolytes;[39] Xiaowei et al. tailored a metal−organic framework (MOF) membrane on the Mg surface and the as-constructed MOF membrane realized selective Mg^{2+} transport.[40] Nonetheless, the synthesis methods of the functional layers mentioned above are complex and costly. The functional layer of metal(M)/$MgCl_2$ by simple displacement reactions of Mg with MCl_2/ether (M = Sn, Bi, etc.) is also a promising way to protect the Mg anode, such as Bi/$MgCl_2$ and Sn/$MgCl_2$.[41−45] Although a much better Mg plating/stripping performance can be achieved, the overpotential for Mg plating/stripping is affected by the residual pores formed during the preparation of the functional layer. More importantly, the long-term cycling stability is severely hampered by the frangibility of the functional layer since the M/$MgCl_2$ layer tends to be pulverized and invalidated during the charge−discharge process, and even during the preparation process, causing the failure of the protection. Although the addition of self-repair additives, such as $GeCl_4$, can repair the broken functional layer, the added Cl^- will change the electrolyte compositions, resulting in cathode kinetics limitation brought about by the Mg−Cl bond and Cl corrosion problem.[46] Therefore, the structure of these functional layers needs to be reconsidered to improve the Mg plating/stripping behavior.

Herein, polytetrahydrofuran (PTHF) is introduced by an in situ THF polyreaction to strengthen the functional layer of Bi/$MgCl_2$ during the displacement reaction. The introduction of PTHF plays multifunctional roles in the functional layer. First, it binds the hybrid functional layer to the Mg substrate and maintains their structural integrity, which is beneficial to buffer the volume change effect caused by the Mg plating/stripping process. Second, the PTHF formed by the in situ THF polyreaction not only inhibits the uncontrollable growths of Bi and $MgCl_2$ particles but also fills the pores formed during the reaction of Mg with $BiCl_3$, making the functional layer more effective. As a result, compared to the simply modified Bi/$MgCl_2$ functional layer, the Bi/$MgCl_2$/PTHF hybrid functional layer shows a lower polarization voltage and a much longer lifespan in Mg symmetrical cells using the conventional $Mg(TFSI)_2$/DME electrolyte. A steady cycling performance is also achieved in Mo_6S_8/Mg full batteries with the designed hybrid functional layer. Furthermore, it is worth noting that the functional layer can still work in the electrolyte with the addition of 2500 ppm H_2O, proving its extraordinary moisture resistance property.

2. RESULTS AND DISCUSSION

To solve the fragile problem of the functional layer, introducing a polymer into the functional layer is an effective strategy to enhance the structure stability. It is worth noting that the polymers cannot contain any hydroxyl, carbonyl, or other groups that can react with Mg metal, and thus PTHF was chosen as the studied polymer in this work. The PTHF in the hybrid functional layer is in situ polymerized from the THF solvent and initiated by $MgCl_2$ or $BiCl_3$ during the reaction between Mg and $BiCl_3$. To accelerate the polyreaction of THF, a small amount of epichlorohydrin (ECH) is necessary to be added into the $BiCl_3$/THF solution. As illustrated in Figure 1, the Mg-Bi@PTHF electrodes were obtained by dropping $BiCl_3$/THF solution containing a small amount of ECH on polished Mg while the blank Mg-Bi electrode samples were obtained by dropping an equivalent amount of $BiCl_3$/THF solution without ECH. During the Mg plating/stripping process, the functional layer on Mg-Bi@PTHF electrodes is expected to maintain its own structural stability due to the presence of PTHF polymers, while that on the Mg-Bi electrodes is easy to be pulverized and invalidated. The possible reaction mechanism of the formation of the hybrid functional layer is illustrated in Figure S1. In reaction 1, $BiCl_3$ is reduced by Mg to produce Bi and $MgCl_2$. Meanwhile, in reactions 2 and 3, $MgCl_2$ acts as a nucleophile and $BiCl_3$ acts as a Lewis acid, respectively, that can initiate the ring-opening of ECH. The intermediate formed by ring-opening continues to initiate the ring-opening of THF and produce PTHF eventually. The introduction of PTHF by an in situ THF polyreaction during the displacement reaction is beneficial to the formation of homogeneous polymers, leading to a better mechanical stability and improved electrochemical performance.

https://doi.org/10.1021/acsami.2c11911
ACS Appl. Mater. Interfaces XXXX, XXX, XXX−XXX

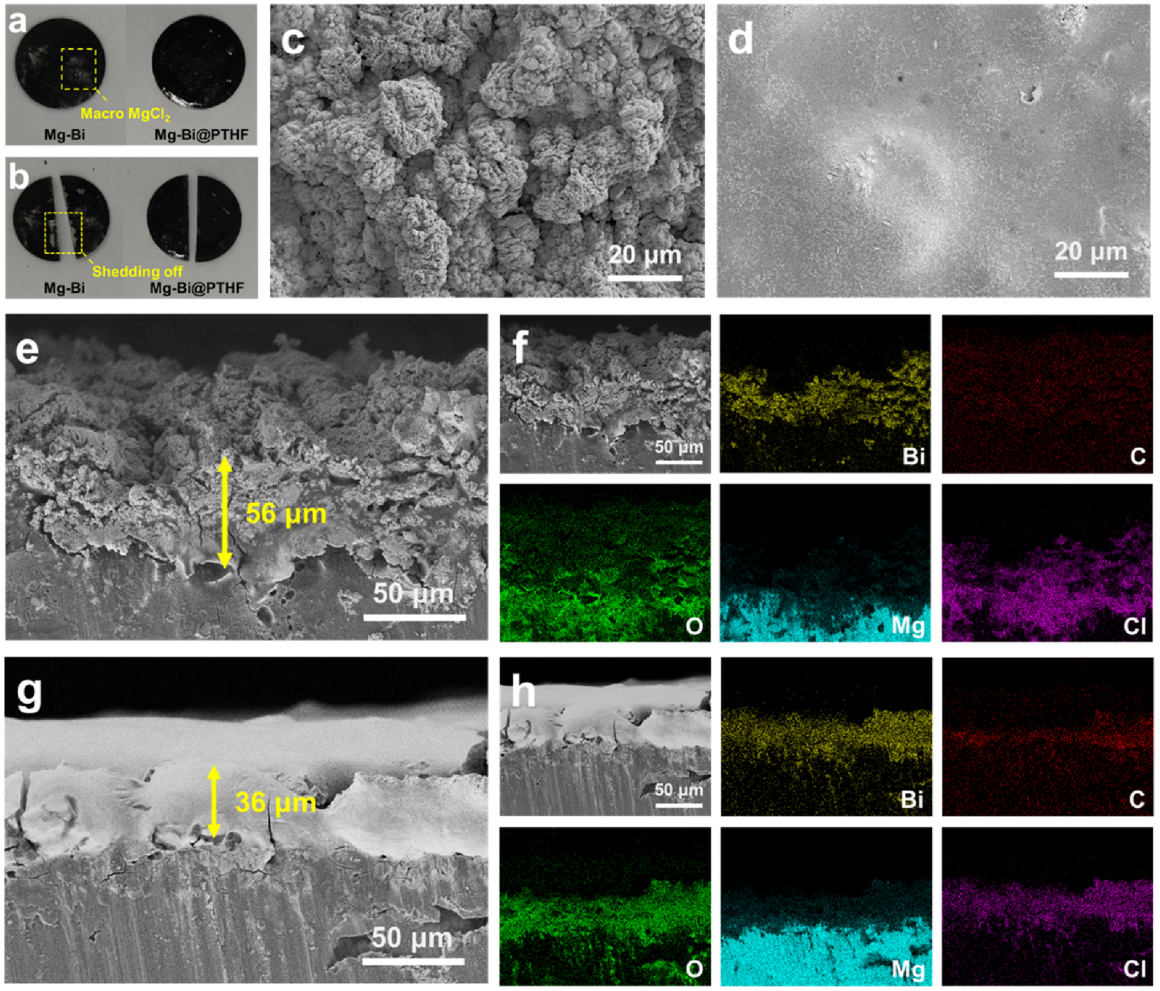

Figure 2. (a) Optical images of Mg-Bi and Mg-Bi@PTHF electrodes. (b) Optical images of Mg-Bi and Mg-Bi@PTHF electrodes' cut pieces. Surface SEM images of the (c) Mg-Bi electrode and (d) Mg-Bi@PTHF electrode. (e) Cross-sectional SEM image and (f) EDS mapping of the Mg-Bi electrode. (g) Cross-sectional SEM image and (h) EDS mapping of the Mg-Bi@PTHF electrode.

Figure 2a shows the optical images of Mg-Bi and Mg-Bi@PTHF electrodes. The functional layer on the Mg-Bi electrode surface is distributed unevenly because the reaction between $BiCl_3$ and Mg is rapid and uncontrollable. $MgCl_2$ is precipitated as macrocrystals, reducing the uniformity of the functional layer. By contrast, the hybrid functional layer on the Mg-Bi@PTHF electrode is more homogeneously distributed without $MgCl_2$ macrocrystals. The uniform distribution of $MgCl_2$ is favorable to the plating/stripping of Mg since Cl^- can inhibit passivation through adsorbing on the electrochemical surface and shielding the attack of H_2O contaminants.[47] To illustrate the mechanical strength of the functional layer with and without PTHF, the Mg-Bi and Mg-Bi@PTHF electrodes were cut into two pieces and the optical images are shown in Figure 2b. The functional layer near the incision of the Mg-Bi electrode pulverizes and falls off while that of the Mg-Bi@PTHF electrode is still attached to the Mg substrate firmly, which is attributed to the binding effect of PTHF polymers. The good mechanical strength of the functional layer is conducive to its structural stability and adhesion to the Mg substrate during the charge−discharge process. Figure 2c,e shows the surface and cross-sectional SEM images of Mg-Bi electrodes, respectively. The functional layer on the Mg-Bi surface appears as a stack of 10 micron-sized Bi secondary particles with a lot of interstices within the layer. The existence of the plentiful interstices is unfavorable to the combination of the functional layer with Mg metal and the electron insulation between the electrolyte and anode. In addition, it can be clearly seen in Figure S3 that macro $MgCl_2$ crystals aggravate the uneven nature of the functional layer. Figure 2d shows the surface SEM image of Mg-Bi@PTHF electrodes. The polymers wrap the Bi particles and fills up the interstice within the layer, so their functional layers are less likely to be pulverized or fall off. It can be seen from Figure 2g that the thickness of the functional layer on the Mg-Bi@PTHF surface is thinner than that on Mg-Bi, mainly due to the presence of PTHF polymers limiting the natural expansion of the functional layer. According to the EDS mapping in Figure 2f,h, Bi and Cl elements are more uniformly distributed within the hybrid functional layer of Mg-Bi@PTHF.

Figure 3a shows the X-ray diffraction (XRD) patterns of Mg-Bi and Mg-Bi@PTHF electrodes. Bi_2Mg_3 and Bi are present in both Mg-Bi and Mg-Bi@PTHF electrodes. According to Table S1, the full-width at half of maximum (FWHM) values of the XRD pattern of Bi on Mg-Bi@PTHF electrodes are generally larger, indicating a decrease in the crystallinity and particle size of Bi. The main reason for such phenomenon is that Bi particles grow too rapidly to produce new crystal nuclei when Mg reacts with $BiCl_3$/THF solution without ECH. After adding ECH into $BiCl_3$/THF solution, THF polymerizes

https://doi.org/10.1021/acsami.2c11911
ACS Appl. Mater. Interfaces XXXX, XXX, XXX−XXX

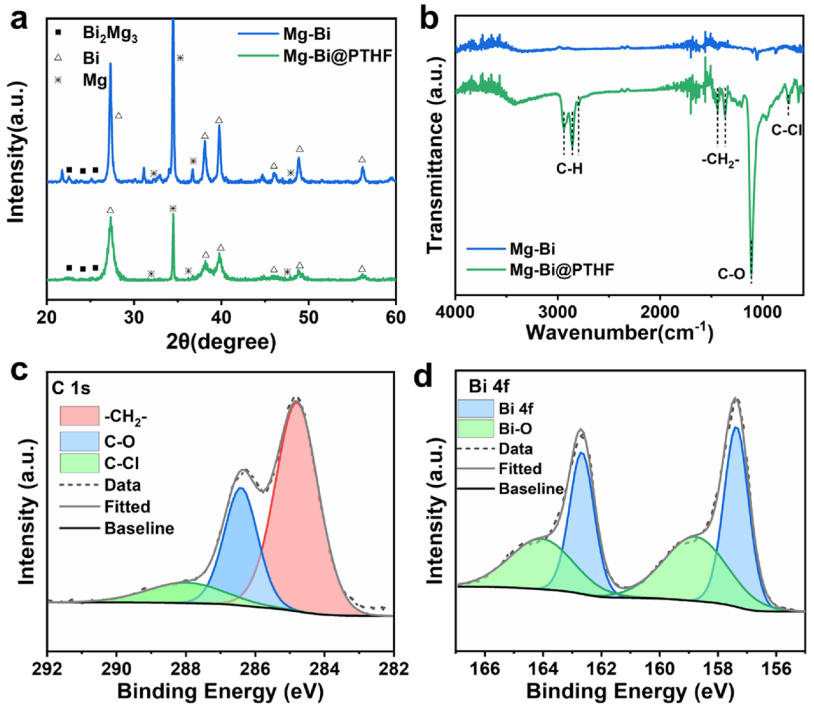

Figure 3. (a) XRD patterns of Mg-Bi and Mg-Bi@PTHF electrodes. (b) ATR-FTIR spectra of Mg-Bi and Mg-Bi@PTHF electrodes. High-resolution XPS (c) C 1s and (d) Bi 4f spectra of Mg-Bi@PTHF electrodes.

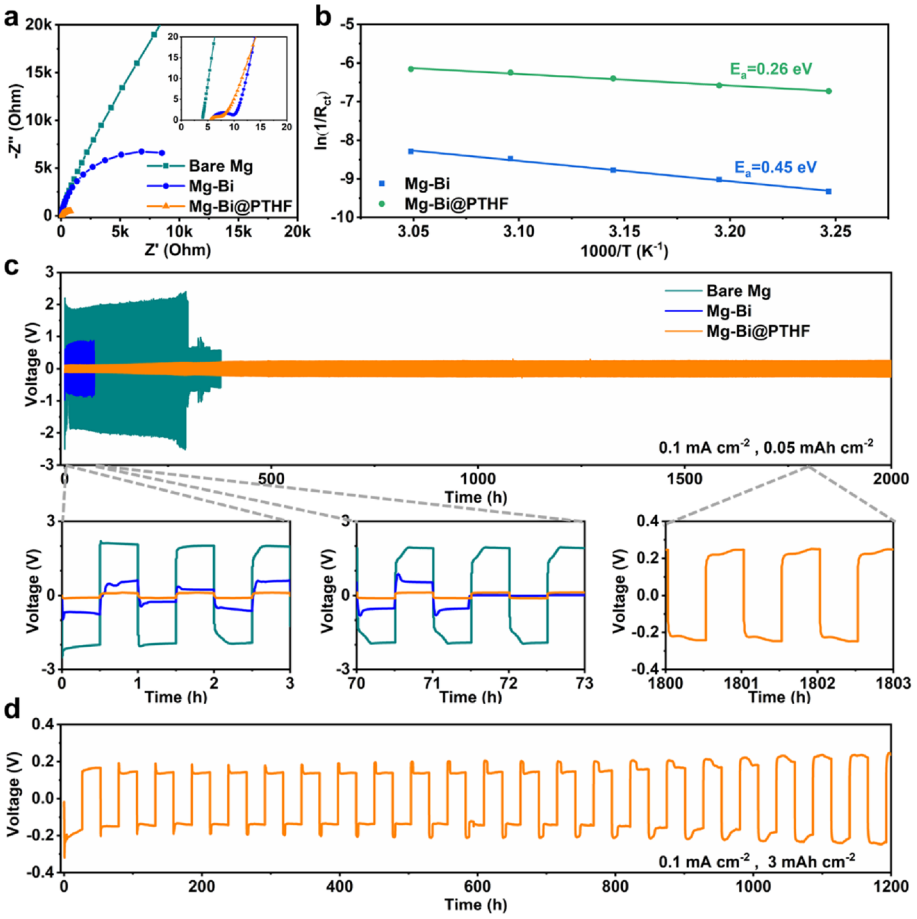

Figure 4. (a) EIS spectra of bare Mg, Mg-Bi, and Mg-Bi@PTHF symmetric cells (0.5 M $Mg(TFSI)_2$/DME). (b) Arrhenius plot of 1/interfacial resistance ($1/R_{ct}$) versus $1000/T$ of Mg-Bi and Mg-Bi@PTHF symmetric cells. Galvanostatic voltage profiles of Mg symmetric cells of bare Mg, Mg-Bi, and Mg-Bi@PTHF at (c) 0. 1 mA cm^{-2}, 0.05 mAh cm^{-2} and (d) 0.1 mA cm^{-2}, 3 mAh cm^{-2}.

https://doi.org/10.1021/acsami.2c11911
ACS Appl. Mater. Interfaces XXXX, XXX, XXX−XXX

rapidly and hinders the further growth of Bi particles during a single displacement reaction. When the growth of Bi particles is limited, Bi tends to produce new crystal nuclei, thus reducing the size of Bi particles. Smaller particles bring a larger specific surface area and more depositional active sites, accelerating the kinetics of the electrochemical reaction. Figure 3b shows the attenuated total reflection Fourier transform infrared (ATR-FTIR) spectra of Mg-Bi and Mg-Bi@PTHF electrodes. Mg-Bi@PTHF has obvious IR absorption peaks compared with Mg-Bi due to the existence of PTHF. The strong peaks at 1108 and 957 cm^{-1} are the C−O asymmetric and symmetric stretching vibration peaks of C-O-C, respectively, which are the characteristic peaks of chain ether. The existence of the C−O stretching vibration characteristic peak of chain ether proves the existence of PTHF polymers. Figure 3c,d shows the high-resolution X-ray photoelectron spectroscopy (XPS) spectra of Mg-Bi@PTHF. In Figure 3d, the XPS peaks at 286.41 and 284.80 eV represent C−O and -CH_2-, respectively. In agreement with previous test results, a large amount of PTHF exists on the Mg-Bi@PTHF surface. In Figure 3d, massive Bi is detected according to the XPS peaks at 157.37 and 162.67 eV. The small amount of Bi_2O_3 mainly comes from oxidation during sample transfer.

To evaluate the electrochemical performance of modified electrodes in conventional electrolytes, bare Mg, Mg-Bi, and Mg-Bi@PTHF symmetrical cells were assembled with the 0.5 M $Mg(TFSI)_2$/DME electrolyte. The electrochemical impedance spectra (EIS) of the three symmetric cells are shown in Figure 4a. The charge transfer resistance of the bare Mg cell reaches 148 kΩ, while that of the Mg-Bi cell decreases to 16 kΩ due to the presence of a simple functional layer. In contrast, Mg-Bi@PTHF reduced the charge transfer resistance to 1 kΩ. Compared with Mg-Bi@PTHF, the larger charge transfer resistance of Mg-Bi symmetric cells implies that the functional layer is not bound firmly with the Mg substrate. One "small semicircle", representing the resistance of charge carrier transport through the interphase, can be seen in the high frequency region of Nyquist plots for Mg-Bi and Mg-Bi@PTHF. It implies that both Mg-Bi and Mg-Bi@PTHF form a stable and efficient interface between the functional layer and electrolyte. As the temperature increases, the R_{ct} decreases, as shown in Figure S4a,b. The equivalent circuit and fitting parameters of R_{ct} are presented in Figure S4c and Table S2. According to Arrhenius' formula, the energy barrier for the charge transport of the functional layer can be calculated from the trends of interfacial resistance with temperature. After PTHF polymers were introduced into the functional layer, the charge transfer activation energy of Mg-Bi@PTHF dropped significantly from 0.45 to 0.26 eV (Figure 4b). The lower charge transfer energy barrier for Mg^{2+} indicates that Mg^{2+} has a more favorable charge transfer process in this functional layer containing PTHF, which is favorable to the improvement of the electrochemical performance of batteries.

Figure 4c exhibits the electrochemical performance of bare Mg, Mg-Bi, and Mg-Bi@PTHF electrodes in symmetric cells at a constant current density of 0.1 mA cm^{-2}. For the bare Mg symmetric cell, a large voltage polarization above 2 V is observed, which is responsible for the failure of the Mg metal batteries. In addition, the polarization voltage decreases during the first several cycles, implying the instability of the interphase on bare Mg. After cycling for 300 h, the polarization voltage of the bare Mg symmetric cell drops sharply to almost 0 V, indicating that a short circuit occurs inside the battery. For the Mg-Bi electrodes that were prepared with 50 μL 0.3 M $BiCl_3$/THF solution, the presence of functional layer decreases its polarization voltage to about 0.4 V. However, the cycling life of the Mg-Bi symmetric cell is not improved, and a short circuit occurs at about 70 h. The reason for the short circuits may be that the functional layer is partially shed from the Mg substrate due to expansion/shrinkage during the Mg plating/stripping process, and Mg can only be plated on certain areas where the hybrid functional layer is attached to the substrate. The uneven distribution of current density accelerates the short circuit, which even causes a shorter lifespan than pure Mg. The polarization voltage of the Mg-Bi electrodes is related to the concentration of $BiCl_3$. As shown in Figure S5, the polarization voltage of Mg-Bi electrodes prepared by 50 μL of 0.1 M $BiCl_3$/THF is 0.5 V, and short circuits occurred after 20 h cycling. As for Mg-Bi electrodes prepared by 50 μL of 0.2 M $BiCl_3$/THF, the polarization voltage slightly decreased to 0.45 V and the lifespan increased to 30 h. Therefore, Mg-Bi electrodes that were prepared with 50 μL of 0.3 M $BiCl_3$/THF solution were chosen in the following study.

The PTHF polymer formed by the addition of ECH has a significant effect on the improvement of electrochemical performance. When 3 vt % ECH was added to 50 μL of 0.3 M $BiCl_3$/THF solution, the polarization voltage of the Mg-Bi@PTHF symmetric cell decreases to about 0.25 V and the cycling life increased to more than 2000 h at 0.1 mA cm^{-2}(Figure 4c). Although the Mg plating potential increased slightly, the overpotential remained below 0.3 V. In the charge and discharge conditions of 0.1 mA cm^{-2} and 3 mAh cm^{-2}, as shown in Figure 4d, the Mg-Bi@PTHF symmetric cells still have a low polarization voltage of 0.2 V and a long lifespan of 2000 h. The decrease in polarization voltage is mainly linked to the introduction of PTHF. PTHF not only binds the functional layer to the Mg substrate more extensively but also makes Bi particles have a larger specific surface area and fill the functional layer with $MgCl_2$-containing polymers. As shown in Figure S5, Mg-Bi@PTHF electrodes prepared by a lower Bi content solution (0.1 M and 0.2 M $BiCl_3$/THF + 3 vt % ECH) have a lower polarization voltage and a longer lifespan than Mg-Bi electrodes prepared by equivalent Bi content solution. It also can be seen that varying the Bi content has a great influence on the electrochemical performance of Mg-Bi and Mg-Bi@PTHF electrodes. When the amount of $BiCl_3$ is reduced, the cycling life of the symmetric cells is shortened, and the polarization voltage is slightly increased. The increase in polarization voltage is caused by the decrease in surface area. As for the shortening of cycling life, we speculate that the increase in Bi content can make the functional layer store more Mg in the form of Bi_2Mg_3 or Mg. However, some of the Bi_2Mg_3 and Mg species become irreversible and accumulate during cycling. A thicker functional layer buffers more "dead Mg" within the layer and prevents them from piercing the separator.

To verify the mechanism of Mg plating, first, we tried to investigate whether the hybrid functional layer stores Mg in the form of Bi_2Mg_3 or Mg. An alloying plateau at about 0.2 V vs Mg^{2+}/Mg would be seen as previously reported if Bi is alloyed to Bi_2Mg_3. However, no obvious capacity is shown at this potential in our galvanostatic voltage profile, indicating that the alloy process is negligible. The plating form of Mg can also be speculated from the plating/stripping capacity. For the Mg-Bi@PTHF electrodes prepared by 50 μL of 0.3 M $BiCl_3$/THF + 3 vt % ECH solution, the theoretical capacity is 1.2 mAh

https://doi.org/10.1021/acsami.2c11911
ACS Appl. Mater. Interfaces XXXX, XXX, XXX−XXX

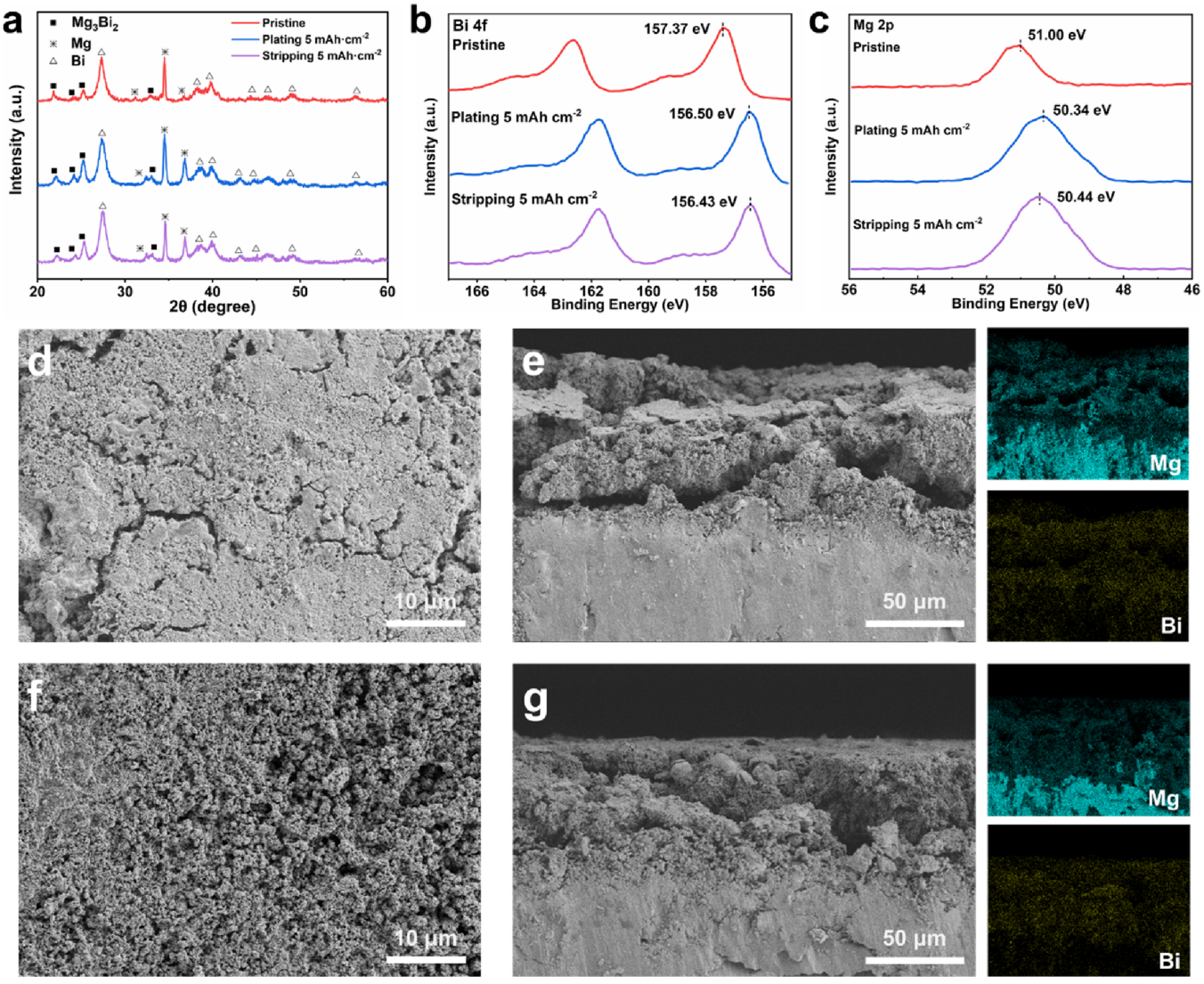

Figure 5. (a) XRD patterns of Mg-Bi@PTHF electrodes at different Mg plating/stripping stages. High-resolution XPS (b) Bi 4f and (c) Mg 2p spectra of Mg-Bi@PTHF electrodes at different Mg plating/stripping stages. (d) Surface and (e) cross-sectional SEM images of Mg-Bi@PTHF at 5 mAh cm^{-2} Mg plating. (f) Surface and (g) cross-sectional SEM images of Mg-Bi@PTHF at 5 mAh cm^{-2} Mg further stripping after 5 mAh cm^{-2} plating.

cm^{-2} if all the Bi reduced from $BiCl_3$/THF solution stores Mg in the form of Bi_2Mg_3. The galvanostatic voltage profile in Figure 4d exhibits that the Mg-Bi@PTHF electrodes can achieve a low overpotential and long cycling life with a higher capacity (0.1 mA cm^{-2}, 3 mAh cm^{-2}), implying the higher probability of Mg being stored in the interstice of Bi layers in the form of Mg metal. To further verify this assumption, the Mg-Bi@PTHF electrodes after Mg plating of 5 mAh cm^{-2} and further stripping of equivalent capacity were characterized by XRD (Figure 5a). The characteristic peaks of Bi have no significant change during Mg plating/stripping, implying that most of the Bi species in the hybrid functional layer would not transform into Bi_2Mg_3 during cycling. Meanwhile, the XRD characteristic peaks of Mg and Bi_2Mg_3 increased after the plating of Mg. According to the galvanostatic voltage profile, Bi_2Mg_3 is probably formed by a chemical reaction between Mg and Bi on the surface of Bi particles rather than an electrochemical reaction. The characteristic peaks of Mg decreases after Mg stripping, but Bi_2Mg_3 is basically unchanged, suggesting that there is still an amount of irreversible Bi_2Mg_3 within the hybrid functional layer that would not transform back to Bi. A high potential of >0.3 V vs Mg^{2+}/Mg is needed to realize the de-alloying reaction, but when the potential that we obtained in cells does not reach this, a de-alloying reaction will not happen. XPS is a powerful characterization technique for surface analysis with an analysis depth of about 10 nm. Figure 5b,c, respectively, shows the XPS Bi 4f and Mg 2p spectra of Mg-Bi@PTHF electrodes at different Mg plating/stripping stages. After Mg plating, the characteristic peaks of Bi and Mg shifted to a lower binding energy, and no obvious shift back was observed after stripping, also indicating that some alloyed Bi and plated Mg on the surface were irreversible. Figure 5d–g shows the SEM images of Mg-Bi@PTHF at different Mg plating/stripping stages. As shown in Figure 5d, Mg plating leads to an increase in Mg content in the hybrid functional layer. Meanwhile, in Figure 5f, after the stripping of Mg, the Mg content in the hybrid functional layer decreased and the Mg substrate was partially dissolved to compensate for the irreversible Bi_2Mg_3, which is consistent with the XRD and XPS results.

https://doi.org/10.1021/acsami.2c11911
ACS Appl. Mater. Interfaces XXXX, XXX, XXX−XXX

Plating of Mg was initially considered to be dendrite-free. Nevertheless, in recent years, more and more research studies have pointed out that the morphology of deposited Mg is influenced by electrolyte properties and current density.[48,49] In the $Mg(TFSI)_2$/DME electrolyte, the 3D growth of plated Mg can still cause a short circuit within a battery.[50] To investigate the Mg plating behavior of Mg electrodes before and after modification, the Mg plating process on bare Mg, Mg-Bi, and Mg-Bi@PTHF was observed by an optical microscope at a current density of 1.0 mA cm^{-2} (Figure 6a). The surface of

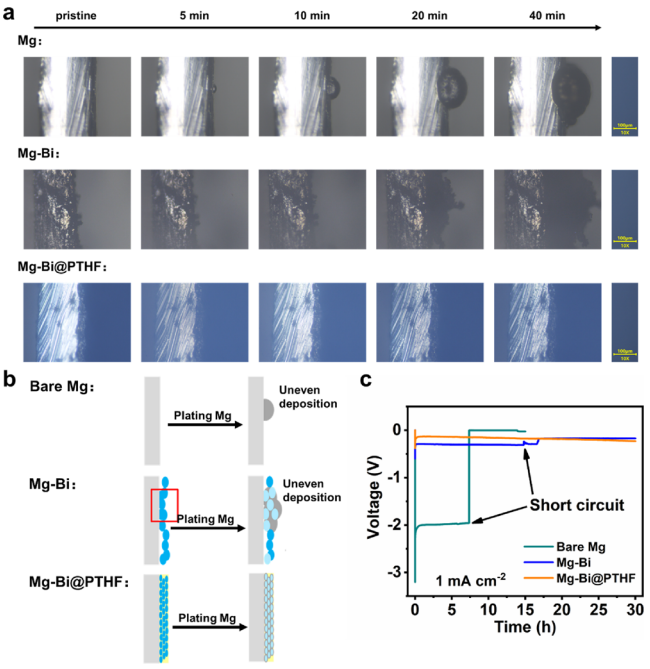

Figure 6. (a) Optical microscopy photographs taken with the increasing electroplating time of the bare Mg, Mg-Bi, and Mg-Bi@PTHF at 1 mA cm^{-2}. (b) Illustration of bare Mg, Mg-Bi, and Mg-Bi@PTHF deposition behavior. (c) Voltage profiles of bare Mg, Mg-Bi, and Mg-Bi@PTHF galvanostatic deposition at a current density of 1.0 mA cm^{-2}.

bare Mg is passivated mostly, and Mg nucleates on certain points where the passivation film is thinner. Eventually, as illustrated in Figure 6b, most Mg plated on the nucleation sites and formed spherical morphology growing along 3D, causing a short circuit. For the Mg-Bi electrode, the functional layer sheds and falls with the gradually increasing magnesium plating amount. On the contrary, no obvious uneven plating morphology or functional layer shedding was observed during the galvanostatic deposition process for Mg-Bi@PTHF. The lifetime of cells (Figure 6c) confirms the Mg plating behavior above. The bare Mg cell will short circuit after galvanostatic deposit for 7 h. For the Mg-Bi electrodes, the lifespan is extended to 15 h. As for Mg-Bi@PTHF, Mg can plate without short circuit for more than 30 h.

To evaluate the practicability of Mg-Bi@PTHF electrodes in Mg metal batteries, Mo_6S_8/Mg full batteries were assembled. When the Mo_6S_8 electrode was matched with bare Mg electrodes, the battery exhibited a large overpotential of 0.81 V and a short lifespan of 24 cycles due to severe passivation and uneven deposition of the Mg anode (Figure 7a and Figure S7a). After replacing the anode with Mg-Bi electrodes, as shown in Figure 7b and Figure S7b, the overpotential of the cell is reduced to 0.50 V. However, in the 33rd cycle, a short circuit still occurred inside the cell due to uneven deposition on the Mg-Bi electrode. When the Mg-Bi@PTHF electrode is used as the anode, as shown in Figure 7c, the cell presented a steady capacity and a reduced overpotential of 0.24 V. In addition, the performance of the Mg-Bi@PTHF/Mo_6S_8 cell remains good within 500 cycles and it shows a capacity retention of 76% after 500 cycles (Figure 7d), verifying the practicability of Mg-Bi@PTHF electrodes in full batteries.

To prove the effectiveness of the hybrid functional layer on Mg-Bi@PTHF in a more rigid test, a little amount of water was added into the 0.5 M $Mg(TFSI)_2$/DME electrolyte. The water content of the electrolyte is 2500 ppm according to Karl-Fischer titration. The addition of water to the electrolyte significantly influenced the performance of the Mg metal, as shown in Figure 7e, resulting in the voltage polarization increase to above 6 V with a short lifespan of 1.3 h due to severe side reactions. For the symmetric cell of the Mg-Bi electrode, the water in the electrolyte also caused a higher polarization voltage (about 0.5 V) and shorter lifespan (25 h) due to irreversible Mg plating and side reactions (Figure 7f). As a comparison, Mg-Bi@PTHF exhibits an outstanding performance with a low polarization voltage of 0.2−0.3 V and a long lifespan of 265 h due to the introduction of PTHF, which is an effective barrier between Mg and water. As shown in Figure S8, the electrolyte and water wettability of Mg-Bi and Mg-Bi@PTHF electrodes was investigated by contact angle measurements to explain this phenomenon. Apparently, the Mg-Bi@PTHF electrodes have a smaller contact angle (9.7°) with the electrolyte and a larger contact angle (33.5°) with water, suggesting that Mg-Bi@PTHF has a better electrolyte wettability and hydrophobicity.

Based on the experimental results above, first, we speculate the mechanism of Mg plating on the Mg-Bi@PTHF electrode. Due to the poor diffusion kinetics of Mg^{2+}, Bi cannot store most Mg in alloy form. Most Mg is plated on the surface of Bi particles, and only negligible amount of plated Mg can form the Bi_2Mg_3 alloy phase on the surface of Bi particles and become irreversible. Because of the high specific surface area of the Bi particles in the hybrid functional layer, the overpotential and short circuit possibility of the Mg-Bi@PTHF electrode are lower than those of bare Mg. Then, the function of PTHF is discussed from two aspects mainly. On the one hand, during the formation process of the hybrid functional layer, PTHF hinders the growth of Bi particles to obtain a higher electrochemically active specific surface area and makes $MgCl_2$ distribute uniformly within the polymers rather than be crystallized. On the other hand, PTHF binds Bi particles together and buffers the expansion/shrinkage of the hybrid functional layer, preserving its structural integrity during the charging−discharging process. PTHF even has a certain hydrophobic effect to protect Mg from the attack of H_2O, ensuring the normal cycling of batteries in a humid environment.

3. CONCLUSIONS

In summary, by introducing the in situ THF polyreaction to the functional layer of Bi/$MgCl_2$ during the displacement reaction, a hybrid functional layer containing Bi, PTHF polymers, and $MgCl_2$ is tailored on the surface of Mg. Compared with the modified Mg electrodes prepared by a simple reaction with $BiCl_3$/THF solution, the hybrid functional layer made by this method exhibits less possibility to be

https://doi.org/10.1021/acsami.2c11911
ACS Appl. Mater. Interfaces XXXX, XXX, XXX−XXX

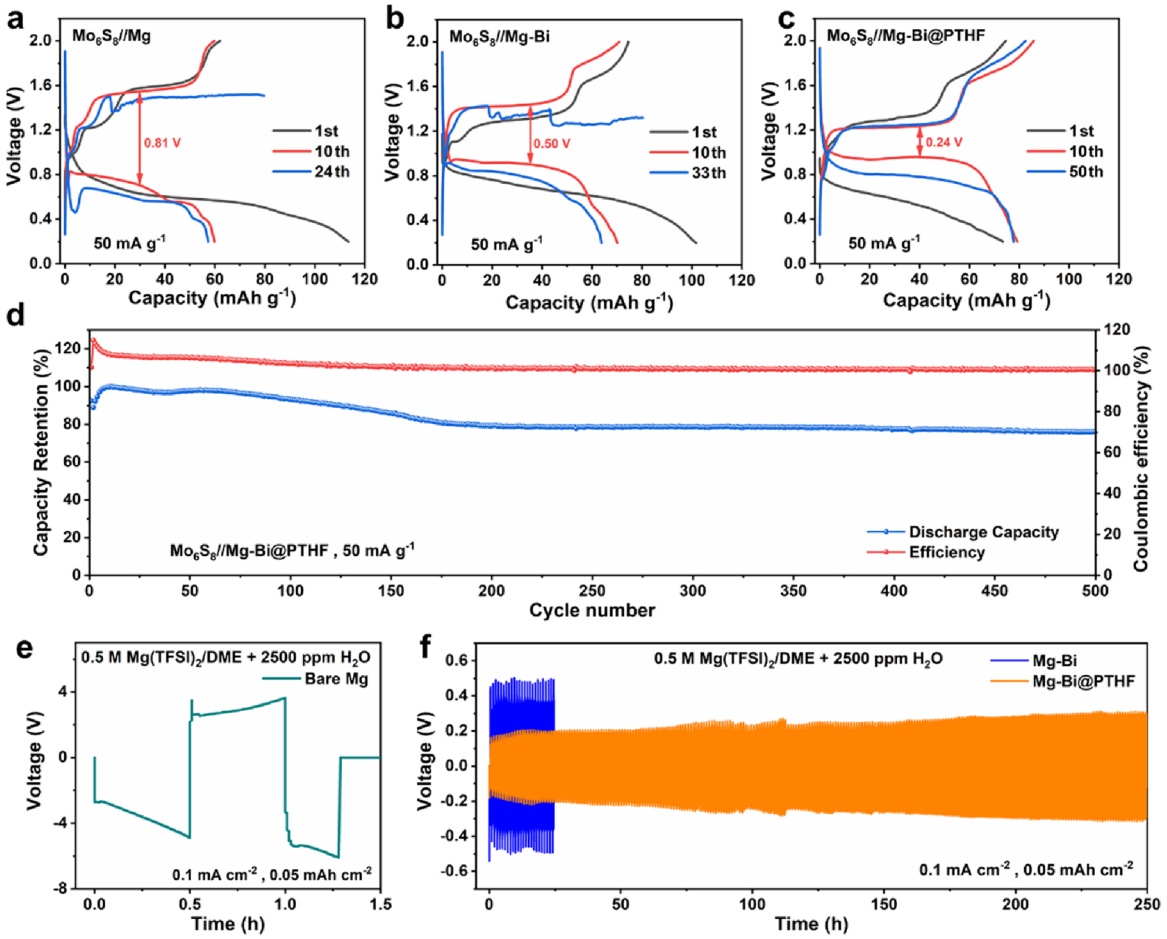

Figure 7. Charge/discharge profiles of the Mg/Mo_6S_8 full batteries with (a) bare Mg, (b) Mg-Bi, and (c) Mg-Bi@PTHF electrodes at 50 mA g^{-1}. (d) Cycling performance of the Mo_6S_8/Mg full batteries with Mg-Bi@PTHF electrodes at 50 mA g^{-1} (using the maximum capacity as 100%). Galvanostatic voltage profiles of Mg symmetric cells of (e) bare Mg, (f) Mg-Bi, and Mg-Bi@PTHF electrodes (0.5 M $Mg(TFSI)_2$/DME+2500 ppm H_2O, 0.1 mA cm^{-2}, 0.05 mAh cm^{-2}).

pulverized or invalidated and possesses a higher electrochemically active specific surface area. Therefore, the polarization voltage of symmetric cells decreases to about 0.25 V and the cycling life reaches more than 2000 h at a current density of 0.1 mA cm^{-2}. The improved electrochemical performance was attributed to the introduction of PTHF, and the roles of PTHF are as follows: (1) During the $BiCl_3$ reduction reaction, the existence of PTHF polymers made the Bi particles smaller and have a higher specific surface area, reducing the overpotential of Mg plating and alleviating the phenomenon of uneven deposition morphology during Mg plating. (2) The PTHF polymers bind the hybrid functional layer and Mg substrate firmly so the hybrid functional layer does not easy fall off partially. The current density distribution on Mg-Bi@PTHF is more uniform compared with bare Mg or Mg-Bi. (3) The Cl^- ions that distributed uniformly within the hybrid functional layer can inhibit passivation through adsorbing to the surface and shielding the attack of H_2O contaminants, which is beneficial for the low overpotential and long-term Mg plating/stripping in the functional layer. This study shows promising applications for the development of Mg metal batteries, providing a facile and effective method to prepare a practical Mg metal anode that can enhance the performance of Mg batteries with conventional electrolytes.

4. EXPERIMENTAL SECTION

4.1. Fabrication of the Functional Layer. Mg foils were polished with 2000 mesh sandpaper to remove the oxides on the surface. Then, the polished Mg foils were punched into small disks with a diameter of 12 mm. A 50 μL 0.3 M $BiCl_3$/THF + 3 vt % ECH solution was dropped onto the surface of Mg disks. After several hours, a black coating was obtained on the Mg surface. Residual $BiCl_3$ on the surface of the Mg electrodes was washed by immersing them in DME solvent. After drying overnight, Mg-Bi@PTHF electrodes were obtained. The Mg-Bi electrodes were prepared by the same way except adding ECH to $BiCl_3$/THF solution. These above processes were carried out in an Ar-filled glove box with both water and oxygen levels below 0.5 ppm.

4.2. Preparation of the 0.5 M $Mg(TFSI)_2$/DME Electrolyte. In Ar-filled glove box with both water and oxygen levels below 0.5 ppm, magnesium bis(trifluoromethanesulfonyl)imide ($Mg(TFSI)_2$, 99.5%, DoDoChem) was dissolved in 1,2-dimethoxyethane (DME, 99%, $H_2O \leq 50$ ppm, Energy) in proportion. The electrolyte was dried by 4 Å molecular sieve (beads, Aladdin) to keep the water level of the electrolyte below 50 ppm (detected by Karl-Fischer titration).

4.3. Preparation of Mo_6S_8 Electrodes. The Mo_6S_8 cathode material was synthesized by using a previously reported method.[S1] The Mo_6S_8 cathode paste was prepared by mixing 80 wt % Mo_6S_8 powders, 10 wt % Super P, and 10 wt % poly(1,1-difluoroethylene) (PVDF) evenly. Then, the cathode paste was cast on small stainless-steel mesh (500 mesh) electrodes with a diameter of 12 mm. The mass loadings of the active Mo_6S_8 were within 1.0−1.5 mg cm^{-2}.

https://doi.org/10.1021/acsami.2c11911
ACS Appl. Mater. Interfaces XXXX, XXX, XXX−XXX

4.4. Material Characterization. Scanning electron microscopy (SEM) and electron energy spectroscopy (EDS) were employed to characterize the morphology and elementary composition of electrodes by a Zeiss GeminiSEM 500 and OXFORD Ultim Extreme. X-ray diffraction (XRD) was conducted by a Rigaku MiniFlex600 (CuKα X-ray). An attenuated total reflectance (ATR) method was carried out in measuring the FTIR spectra with a ThermoFisher IS5 infrared spectrometer. X-ray photoelectron spectroscopy (XPS) was performed by a Thermo Scientific ESCALAB Xi+.

4.5. Electrochemical Performance Test. All cells were assembled in an Ar-filled glove box with both water and oxygen levels less than 0.5 ppm. Symmetrical Mg cells (2032-type coin cells) were assembled by bare Mg or modified Mg electrodes with glass microfiber filter (Whatman GF/D 1823-047) as a separator and 0.5 M $Mg(TFSI)_2$/DME as an electrolyte. A galvanostatic test was performed on a Neware CT-3008 at a current density of 0.1 mA cm^{-2} at room temperature (25 °C) (30 min charging and 30 min discharging). A Solarton 1260/1287A was applied to characterize the electrochemical impedance spectrum of Mg symmetric cells. The data were measured at a frequency range from 1 MHz to 0.01 Hz by applying a sine wave with an amplitude of 10.0 mV. The in situ observation cell was assembled with pure Mg plates or modified Mg plates. The plating behavior on the Mg plates was observed and photographed by an Olympus BX53M system microscope system at a current density of 1 mA cm^{-2}. The modified Mg electrodes were used as the anode, and the Mo_6S_8 electrodes prepared above were used as the cathode to assemble the 2032-type coin cells. The galvanostatic test was performed at a voltage range from 0.2 to 2.0 V, and the current density was 50 mA g^{-1}.

■ ASSOCIATED CONTENT

Supporting Information

The Supporting Information is available free of charge at https://pubs.acs.org/doi/10.1021/acsami.2c11911.

Characterization of materials and electrochemical performance test (possible reaction mechanism, EDS analysis, EDS mapping, FWHM, EIS spectra and equivalent circuit model, fitting parameters of R_{ct}, cycling performance, and contact angle) (PDF)

■ AUTHOR INFORMATION

Corresponding Authors

Jing Zeng − *College of Chemistry and Chemical Engineering, State-Province Joint Engineering Laboratory of Power Source Technology for New Energy Vehicle, State Key Laboratory of Physical Chemistry of Solid Surfaces, Engineering Research Center of Electrochemical Technology, Ministry of Education, Collaborative Innovation Center of Chemistry for Energy Materials, Xiamen University, Xiamen 361005, China*; Email: zengjing@xmu.edu.cn

Jinbao Zhao − *College of Chemistry and Chemical Engineering, State-Province Joint Engineering Laboratory of Power Source Technology for New Energy Vehicle, State Key Laboratory of Physical Chemistry of Solid Surfaces, Engineering Research Center of Electrochemical Technology, Ministry of Education, Collaborative Innovation Center of Chemistry for Energy Materials, Xiamen University, Xiamen 361005, China*; Email: jbzhao@xmu.edu.cn

Authors

Yichao Zhuang − *College of Chemistry and Chemical Engineering, State-Province Joint Engineering Laboratory of Power Source Technology for New Energy Vehicle, State Key Laboratory of Physical Chemistry of Solid Surfaces, Engineering Research Center of Electrochemical Technology, Ministry of Education, Collaborative Innovation Center of Chemistry for Energy Materials, Xiamen University, Xiamen 361005, China*

Dongzheng Wu − *College of Chemistry and Chemical Engineering, State-Province Joint Engineering Laboratory of Power Source Technology for New Energy Vehicle, State Key Laboratory of Physical Chemistry of Solid Surfaces, Engineering Research Center of Electrochemical Technology, Ministry of Education, Collaborative Innovation Center of Chemistry for Energy Materials, Xiamen University, Xiamen 361005, China*

Fei Wang − *College of Chemistry and Chemical Engineering, State-Province Joint Engineering Laboratory of Power Source Technology for New Energy Vehicle, State Key Laboratory of Physical Chemistry of Solid Surfaces, Engineering Research Center of Electrochemical Technology, Ministry of Education, Collaborative Innovation Center of Chemistry for Energy Materials, Xiamen University, Xiamen 361005, China*

Yaoqi Xu − *College of Chemistry and Chemical Engineering, State-Province Joint Engineering Laboratory of Power Source Technology for New Energy Vehicle, State Key Laboratory of Physical Chemistry of Solid Surfaces, Engineering Research Center of Electrochemical Technology, Ministry of Education, Collaborative Innovation Center of Chemistry for Energy Materials, Xiamen University, Xiamen 361005, China*

Complete contact information is available at: https://pubs.acs.org/10.1021/acsami.2c11911

Notes

The authors declare no competing financial interest.

■ ACKNOWLEDGMENTS

The authors gratefully acknowledge the National Natural Science Foundation of China (nos. 21875198, 22005257, and 22021001) and Natural Science Foundation of Fujian Province of China (No. 2020J05009) for financial support.

■ REFERENCES

(1) Choi, J. W.; Aurbach, D. Promise and Reality of Post-Lithium-Ion Batteries with High Energy Densities. *Nat. Rev. Mater.* **2016**, DOI: 10.1038/natrevmats.2016.13.

(2) Massé, R. C.; Uchaker, E.; Cao, G. Beyond Li-ion: Electrode Materials for Sodium- and Magnesium-Ion Batteries. *Sci. China Mater.* **2015**, 715.

(3) Wu, X.; He, G.; Ding, Y. Dealloyed Nanoporous Materials for Rechargeable Post-Lithium Batteries. *ChemSusChem* **2020**, 3287.

(4) You, C.; Wu, X.; Yuan, X.; Chen, Y.; Liu, L.; Zhu, Y.; Fu, L.; Wu, Y.; Guo, Y.-G.; van Ree, T. Advances in Rechargeable Mg Batteries. *J. Mater. Chem. A* **2020**, 25601.

(5) Liu, F.; Wang, T.; Liu, X.; Fan, L. Z. Challenges and Recent Progress on Key Materials for Rechargeable Magnesium Batteries. *Adv. Energy Mater.* **2021**, 2000787.

(6) Pei, C.; Xiong, F.; Yin, Y.; Liu, Z.; Tang, H.; Sun, R.; An, Q.; Mai, L. Recent Progress and Challenges in the Optimization of Electrode Materials for Rechargeable Magnesium Batteries. *Small* **2021**, 2004108.

(7) Mohtadi, R.; Tutusaus, O.; Arthur, T. S.; Zhao-Karger, Z.; Fichtner, M. The Metamorphosis of Rechargeable Magnesium Batteries. *Joule* **2021**, 581.

(8) Song, C.; Shuang, F.; Henan, L.; Yumeng, S.; Hui Ying, Y. Recent Advances in Kinetic Optimizations of Cathode Materials for Rechargeable Magnesium Batteries. *Coord. Chem. Rev.* **2022**, No. 214597.

(9) Li, D.; Yuan, Y.; Liu, J.; Fichtner, M.; Pan, F. A Review on Current Anode Materials for Rechargeable Mg Batteries. *J. Magnesium Alloys* **2020**, 963.
(10) Ran, A.; Michael, S.; Baruch, H.; Yosef, G.; Doron, A. Anode-Electrolyte Interfaces in Secondary Magnesium Batteries. *Joule* **2019**, 27−52.
(11) Ramasubramonian, D.; Brian, J. I.; Reza, S.-Y. Progress in Development of Electrolytes for Magnesium Batteries. *Energy Storage Mater.* **2019**, 136−153.
(12) Muldoon, J.; Bucur, C. B.; Oliver, A. G.; Sugimoto, T.; Matsui, M.; Kim, H. S.; Allred, G. D.; Zajicek, J.; Kotani, Y. Electrolyte Roadblocks to a Magnesium Rechargeable Battery†. *Energy Environ. Sci.* **2012**, 5941.
(13) Mizrahi, O.; Amir, N.; Pollak, E.; Chusid, O.; Marks, V.; Gottlieb, H.; Larush, L.; Zinigrad, E.; Aurbach, D. Electrolyte Solutions with a Wide Electrochemical Window for Rechargeable Magnesium Batteries. *J. Electrochem. Soc.* **2008**, A103.
(14) Vestfried, Y.; Chusid, O.; Goffer, Y.; Aped, P.; Aurbach, D. Structural Analysis of Electrolyte Solutions Comprising Magnesium−Aluminate Chloro−Organic Complexes by Raman Spectroscopy. *Organometallics* **2007**, 3130.
(15) Wan, L. F.; Perdue, B. R.; Apblett, C. A.; Prendergast, D. Mg Desolvation and Intercalation Mechanism at the Mo_6S_8 Chevrel Phase Surface. *Chem. Mater.* **2015**, 5932.
(16) Yoo, H. D.; Shterenberg, I.; Gofer, Y.; Gershinsky, G.; Pour, N.; Aurbach, D. Mg Rechargeable Batteries: an On-Going Challenge†. *Energy Environ. Sci.* **2013**, 2265.
(17) Chakrabarty, S.; Blázquez, J. A.; Sharabani, T.; Maddegalla, A.; Leonet, O.; Urdampilleta, I.; Sharon, D.; Noked, M.; Mukherjee, A. Stability of Current Collectors Against Corrosion in APC Electrolyte for Rechargeable Mg Battery. *J. Electrochem. Soc.* **2021**, No. 080526.
(18) Yagi, S.; Tanaka, A.; Ichikawa, Y.; Ichitsubo, T.; Matsubara, E. Electrochemical Stability of Magnesium Battery Current Collectors in a Grignard Reagent-Based Electrolyte. *J. Electrochem. Soc.* **2013**, C83.
(19) Tutusaus, O.; Mohtadi, R.; Arthur, T. S.; Mizuno, F.; Nelson, E. G.; Sevryugina, Y. V. An Efficient Halogen-Free Electrolyte for Use in Rechargeable Magnesium Batteries. *Angew. Chem.* **2015**, 8011−8015.
(20) Hahn, N. T.; Seguin, T. J.; Lau, K.-C.; Liao, C.; Ingram, B. J.; Persson, K. A.; Zavadil, K. R. Enhanced Stability of the Carba-closo-dodecaborate Anion for High Voltage Battery Electrolytes through Rational Design. *J. Am. Chem. Soc.* **2018**, 11076.
(21) Ha, S.-Y.; Lee, Y.-W.; Woo, S. W.; Koo, B.; Kim, J.-S.; Cho, J.; Lee, K. T.; Choi, N.-S. Magnesium(II) Bis(trifluoromethane sulfonyl) Imide-Based Electrolytes with Wide Electrochemical Windows for Rechargeable Magnesium Batteries. *ACS Appl. Mater. Interfaces* **2014**, 4063.
(22) Keyzer, E. N.; Glass, H. F. J.; Liu, Z.; Bayley, P. M.; Dutton, S. E.; Grey, C. P.; Wright, D. S. Mg(PF6)2-Based Electrolyte Systems: Understanding Electrolyte−Electrode Interactions for the Development of Mg-Ion Batteries. *J. Am. Chem. Soc.* **2016**, 8682.
(23) Shterenberg, I.; Salama, M.; Gofer, Y.; Aurbach, D. Hexafluorophosphate-Based Solutions for Mg Batteries and the Importance of Chlorides. *Langmuir* **2017**, 9472.
(24) Shterenberg, I.; Salama, M.; Yoo, H. D.; Gofer, Y.; Park, J.-B.; Sun, Y.-K.; Aurbach, D. Evaluation of $(CF_3SO_2)2N−(TFSI)$ Based Electrolyte Solutions for Mg Batteries. *J. Electrochem. Soc.* **2015**, A7118.
(25) Rajput, N. N.; Qu, X.; Sa, N.; Burrell, A. K.; Persson, K. A. The Coupling between Stability and Ion Pair Formation in Magnesium Electrolytes from First-Principles Quantum Mechanics and Classical Molecular Dynamics. *J. Am. Chem. Soc.* **2015**, 3411.
(26) Seguin, T. J.; Hahn, N. T.; Zavadil, K. R.; Persson, K. A. Elucidating Non-aqueous Solvent Stability and Associated Decomposition Mechanisms for Mg Energy Storage Applications From First-Principles. *Front. Chem.* **2019**, DOI: 10.3389/fchem.2019.00175.
(27) Yu, Y.; Baskin, A.; Valero-Vidal, C.; Hahn, N. T.; Liu, Q.; Zavadil, K. R.; Eichhorn, B. W.; Prendergast, D.; Crumlin, E. J. Instability at the Electrode/Electrolyte Interface Induced by Hard Cation Chelation and Nucleophilic Attack. *Chem. Mater.* **2017**, 8504.
(28) Bucur, C. B.; Gregory, T.; Oliver, A. G.; Muldoon, J. Confession of a Magnesium Battery. *J. Phys. Chem. Lett.* **2015**, 3578.
(29) Mao-Ling Xie, J. W.; Hu, C.-J.; Zheng, L.; Kong, H.-B.; Shen, Y.-B.; Chen, H.-W.; Chen, L.-W. An Additive Incorporated Non-Nucleophilic Electrolyte for Stable Magnesium Ion Batteries. *J. Electrochem.* **2022**, *28*, 2108561.
(30) Salama, M.; Shterenberg, I.; Shimon, L.; Keinan-Adamsky, K.; Afri, M.; Gofer, Y.; Aurbach, D. Structural Analysis of Magnesium Chloride Complexes in Dimethoxyethane Solutions in the Context of Mg Batteries Research. *J. Phys. Chem. C* **2017**, 24909.
(31) Xin-Cheng, H.; Zhen-Zhen, S.; Jing, W.; Yue-Xian, S.; Bing, L.; Hui-Juan, Y.; Rui, W.; Li-Jun, W. Insight into Interfacial Processes and Degradation Mechanism in Magnesium Metal Batteries. *Nano Energy* **2020**, 105338.
(32) Singyuk, H.; Xiao, J.; Karen, G.; Peng-fei, W.; Luning, W.; Jijian, X.; Ruimin, S.; Oleg, B.; Chunsheng, W. Solvation Sheath Reorganization Enables Divalent Metal Batteries with Fast Interfacial Charge Transfer Kinetics. *Science* **2021**, 172.
(33) Wanyu, Z.; Zhenghui, P.; Yijie, Z.; Yuan, L.; Huanglin, D.; Yayun, S.; Zhijun, Z.; Bowen, Z.; Jianping, C.; Xiaoli, Z.; Yang, X. Tailoring Coordination in Conventional Ether-based Electrolytes for Reversible Magnesium Metal Anodes. *Angew. Chem., Int. Ed.* **2022**, e202205187.
(34) Tuerxun, F.; Yamamoto, K.; Hattori, M.; Mandai, T.; Nakanishi, K.; Choudhary, A.; Tateyama, Y.; Sodeyama, K.; Nakao, A.; Uchiyama, T.; Matsui, M.; Tsuruta, K.; Tamenori, Y.; Kanamura, K.; Uchimoto, Y. Determining Factor on the Polarization Behavior of Magnesium Deposition for Magnesium Battery Anode. *ACS Appl. Mater. Interfaces* **2020**, 25775.
(35) Zhiming, L.; Chunmei, B. Strategies to Enable Reversible Magnesium Electrochemistry: From Electrolytes to Artificial Solid−Electrolyte Interphases. *Angew. Chem., Int. Ed.* **2021**, 11036−11047.
(36) Yue, S.; Fei, A.; Yi-Chun, L. Electrolyte and Interphase Design for Magnesium Anode: Major Challenges and Perspectives. *Small* **2022**, 2200009.
(37) Seoung-Bum, S.; Tao, G.; Steve, P. H.; Steirer, K. X.; Adam, S.; Andrew, N.; Chunsheng, W.; Arthur, C.; Kang, X.; Chunmei, B. An Artificial Interphase Enables Reversible Magnesium Chemistry in Carbonate Electrolytes. *Nat. Chem.* **2018**, 532.
(38) Yaqi, L.; Pengjian, Z.; Ruinan, L.; Hua, H.; Yulin, M.; Chunyu, D.; YunZhi, G.; Geping, Y.; Robert, S. W. Formation of an Artificial Mg2+-Permeable Interphase on Mg Anodes Compatible with Ether and Carbonate Electrolytes. *ACS Appl. Mater. Interfaces* **2021**, 24565.
(39) Holc, C.; Dimogiannis, K.; Hopkinson, E.; Johnson, L. R. Critical Role of the Interphase at Magnesium Electrodes in Chloride-Free, Simple Salt Electrolytes. *ACS Appl. Mater. Interfaces* **2021**, 29708.
(40) Yijie, Z.; Jiang, L.; Wanyu, Z.; Huanglin, D.; Xiaoli, Z.; Yuan, L.; Bowen, Z.; Xiaowei, Y. Defect-Free Metal−Organic Framework Membrane for Precise Ion/Solvent Separation toward Highly Stable Magnesium Metal Anode. *Adv. Mater.* **2021**, 2108114.
(41) Ruijing, L.; Xuze, G.; Jiahua, Z.; Yongyao, X.; Jiayan, L. Enabling Mg Metal Anodes Rechargeable in Conventional Electrolytes by Fast Ionic Transport Interphase. *Nat. Sci. Rev.* **2020**, 333−341.
(42) Yimin, Z.; Aobing, D.; Shanmu, D.; Feng, J.; Ziyang, G.; Xuesong, G.; Xuelian, Q.; Xinhong, Z.; Guanglei, C. A Bismuth-Based Protective Layer for Magnesium Metal Anode in Noncorrosive Electrolytes. *ACS Energy Lett.* **2021**, 2594.
(43) Jiwoong, B.; Hyoju, P.; Xuelin, G.; Xiao, Z.; Jamie, H. W.; Guihua, Y. High-Performance Magnesium Metal Batteries via Switching the Passivation Film into a Solid Electrolyte Interphase. *Energy Environ. Sci.* **2021**, 4391−4399.
(44) Zhang, R.; Cui, C.; Xiao, R.; Ruinan, L.; Mu, T.; Huo, H.; Ma, Y.; Yin, G.; Zuo, P. Enabling the Conventional TFSI-Based Electrolytes for High-Performance Mg/Li Hybrid Batteries by Mg Electrode Interfacial Regulation. *Chem. Eng. J.* **2022**, 136592.
(45) Bingxin, W.; Huanglin, D.; Xiaoli, Z.; Jiahe, W.; Wanyu, Z.; Min, G.; Yijie, Z.; Jinjin, L.; Zi-Feng, M.; Xiaowei, Y. Three-

https://doi.org/10.1021/acsami.2c11911
ACS Appl. Mater. Interfaces XXXX, XXX, XXX−XXX

Dimensional Magnesiophilic Scaffolds for Reduced Passivation toward High-Rate Mg Metal Anodes in a Noncorrosive Electrolyte. *ACS Appl. Mater. Interfaces* **2020**, 28298.
(46) Jiahua, Z.; Xuze, G.; Ruijing, L.; Donghong, W.; Ping, L.; Jiayan, L. Rechargeable Mg Metal Batteries Enabled by a Protection Layer Formed in Vivo. *Energy Storage Mater.* **2019**, 408−413.
(47) Connell, J. G.; Genorio, B.; Lopes, P. P.; Strmcnik, D.; Stamenkovic, V. R.; Markovic, N. M. Tuning the Reversibility of Mg Anodes via Controlled Surface Passivation by H_2O/Cl− in Organic Electrolytes. *Chem. Mater.* **2016**, 8268.
(48) Markus, S. D.; Thomas, D.; Behm, R. J.; Stefano, P.; Guinevere, A. G. Dendrite Growth in Mg Metal Cells Containing $Mg(TFSI)_2$ /Glyme Electrolytes. *J. Electrochem. Soc.* **2018**, A1983.
(49) Rachel, D.; Ankit, V.; David, S.; Feng, H.; Coleman, F.; Sisi, X.; Van Jonathan, B.; Kelvin, X.; Matt, P.; Partha, P. M.; Sarbajit, B. Formation of Magnesium Dendrites during Electrodeposition. *ACS Energy Lett.* **2019**, 375−376.
(50) Janna, E.-R.; Kathleen, M.; Murtaza, Z.; Cary, L. P. Kinetic- versus Diffusion-Driven Three-Dimensional Growth in Magnesium Metal Battery Anodes. *Joule* **2020**, 1324.
(51) Lancry, E.; Levi, E.; Mitelman, A.; Malovany, S.; Aurbach, D. Molten Salt Synthesis (MSS) of $Cu_2Mo_6S_8$—New Way for Large-Scale Production of Chevrel Phases. *J. Solid State Chem.* **2006**, 1879.

https://doi.org/10.1021/acsami.2c11911
ACS Appl. Mater. Interfaces XXXX, XXX, XXX−XXX